THE JOURNAL OF PHYSICAL CHEMISTRY LETTERS
A JOURNAL OF THE AMERICAN CHEMICAL SOCIETY

pubs.acs.org/JPCL

Letter

Tracing Vortex Clustering in a Superconductor by the Magnetic Flux Distribution

A. Vagov* and E.G. Nikonov

Cite This: J. Phys. Chem. Lett. 2023, 14, 3743−3748

Read Online

ACCESS | Metrics & More | Article Recommendations

ABSTRACT: By investigating spatial configurations of the intermediate mixed state in an intertype superconductor, it is shown that vortex clustering can be characterized by the sample averaged distribution of the penetrating magnetic field. The clustering is manifested in the two-peak structure of the distribution. The second peak indicates a spot a material occupies in the phase diagram of superconductivity types. The conclusions are general and do not depend on details of the model.

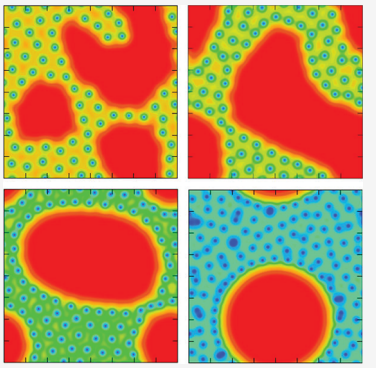

Particle clustering is a broad interdisciplinary phenomenon taking place in a large number of systems in physics as well as in chemistry. Numerous examples include metal clusters, such as homonuclear superatoms,[1−4] ultrastable colloidal semiconductor nanocrystals,[5−9] liquid[10,11] and hybrid organic−inorganic[12] clusters, and can also be found as far as in high-energy physics, e.g., hadrons as clusters of confined quarks and gluons.[13−15] Clustering rearranges the internal structure of matter such that the latter demonstrates qualitatively different characteristics.[1,16−18] Understanding general mechanisms underlying the clustering phenomenon and tracing its details experimentally is thus a problem of fundamental importance.

A special example of clustering is provided by superconducting materials "between" two conventional superconductivity types I and II. Such materials, referred to as type II/1 or as intertype (IT) superconductors,[19,20] reveal properties that attribute them to neither of the two conventional superconductivity types.[21−23] In particular, IT superconductors develop the so-called intermediate mixed state (IMS) that has characteristics of both the mixed state with vortices, specific to type-II materials, and of the intermediate state, found in type-I superconductors, where the normal and superconducting Meissner phases interchange spatially.[19,24,25]

In a mixed state of a superconductor vortices can be regarded as elementary "particles". In a type-II material these "particles" are fully repulsive and form an extended regular periodic structure, known as the Abrikosov lattice. An IT superconductor is characterized by instability of the vortex lattice.[26,27] The periodical vortex structure breaks down, and vortices form the IMS with clusters surrounded by domains of the vortex-free Meissner phase. Remarkably, the shapes and internal structure of the clusters vary substantially. Their structure ranges from a rigid lattice to vortex liquid, and the shape also changes notably, displaying many exotic patterns like elongated vortex molecules and chains.[28]

As in other cluster formation processes, the key to understand properties of the emerging IMS structures lies in details of the interaction between its vortex "particles".[19] Unlike type-II superconductors, vortex−vortex interactions in IT materials is nonmonotonic,[29] being attractive at long ranges and having a minimum at a finite intervortex distance. What is, however, specific to the IMS is a much greater role of the multivortex interactions. Deep in the IT regime, these become dominant ensuring stability of large clusters even if the interaction between two vortices is fully attractive.[29]

Tracing dynamics of the cluster formation while changing system parameters, e.g., magnetic field and temperature, is the most direct way to uncover the clustering mechanism. A complete picture of the clustering is obtained when one traces positions of all particles in the system. However, it is impractical in many cases, and the analysis has to be restricted to studying some integral characteristics of the particle configurations.

In superconductors, vortex positions can be most easily measured at the sample surface,[30] precisely where vortices are

Received: March 17, 2023
Accepted: April 3, 2023

https://doi.org/10.1021/acs.jpclett.3c00721
J. Phys. Chem. Lett. 2023, 14, 3743−3748

most distorted due to their interaction with the surface and the stray fields outside the sample. Moreover, the distortion becomes especially strong in IT materials where the superconducting state is almost degenerate due to the system proximity to the critical Bogomolny point (B-point).[31]

In contrast, measuring small angle neutron scattering (SANS) reveals vortex positions inside a superconducting sample by giving a formfactor of the magnetic flux distribution.[32−34] SANS is essentially equivalent to X-ray measurements of crystal structures and is well-suited to study periodic lattices, characterized by the Bragg peaks in the formfactor. For highly irregular configurations, typical for the IMS, the SANS gives smeared images that are not easy to interpret.[34,35]

Another popular approach to access the magnetic flux inside a material is the muon spin rotation experiment (MSRE),[36] which probes the average value of the flux. The MSRE cannot resolve vortex positions inside a superconductor yielding instead a histogram of the magnetic flux distribution.[37] Seemingly, MSRE provides much less detailed information on the vortex configurations. Nevertheless, the measurements of superconductive ZrB_{12} revealed notable deviations from what is expected for conventional type I/II superconductors.[37] These were interpreted as a signature of the vortex-free Meissner phase presence. In single-band superconductors, it is regarded as a hallmark of the IMS.[33,34]

It is worth noting that the IMS with vortex clusters coexisting with vortex-free Meissner voids can be described theoretically using the two-component Ginzburg−Landau (GL) model,[38] leading to a suggestion ZrB_{12} is a multiband superconductor.[37] It is known, however, that the GL parameter of ZrB_{12} is close to $\kappa_0 = 1/\sqrt{2}$,[39−41] where according to the GL theory, type I and type II superconductivity interchange. This places ZrB_{12} among the so-called low-κ superconductors, in which the spatial profile of the penetrating magnetic flux is known to strongly deviate from the standard Abrikosov lattice.[19,21] Theoretical analysis of such superconductors, based on a conventional single-band Bardeen−Cooper−Schrieffer (BCS) theory with the s-wave pairing, also gives the IMS.[28] It takes place when the system is close to the B-point, where superconductivity types I and II interchange.[20,42] The analysis based on the perturbation expansion demonstrated that the mechanism underlying the IMS is the same in both two- and single-band superconductors.[20,43] In both single- and two-band cases, the defining feature of the IMS is the vortex−vortex interaction being attractive at long distances.[29,38,43]

In this work, we calculate the flux distribution for the IMS of an IT superconductor and investigate its dependence on the average magnetic field in the sample. Results of the calculations reveal the field distribution has peculiar characteristics, which can be reliably used to follow the process of vortex clustering in superconductors. Moreover, its dependence on the average field indicates the place of the material in the phase diagram for superconductivity types.

The analysis is performed using the microscopic BCS model with the s-wave pairing symmetry, which is treated using the perturbation expansion with respect to proximity $\tau = 1 - T/T_c$ to the critical temperature T_c. In this expansion, the gap Δ and the field $\mathcal{B}$ are represented as series

$$\Delta = \tau^{1/2}(\psi + \tau\phi + ...) \quad \mathcal{B} = \tau(\mathbf{B} + \tau\mathbf{b} + ...) \tag{1}$$

The free energy functional is similarly represented as the series expansion. To obtain it one also has to take into account the coordinate scaling $\mathbf{x} \to \mathbf{x}/\sqrt{\tau}$. Substituting these into the BCS expression for the free energy functional, one obtains the leading contribution to the latter as[20]

$$f = \tau^2(f_0 + \tau f_1 + ...) \tag{2}$$

where the lowest-order contribution is the standard result for the GL theory

$$f_0 = \frac{\mathbf{B}^2}{8\pi} + a|\psi|^2 + \frac{b}{2}|\psi|^4 + \mathcal{K}|\mathbf{D}\psi|^2 \tag{3}$$

with $\mathbf{D} = \nabla - i2e\mathbf{A}/(\hbar c)$, and the correction to the GL expression is given as

$$\begin{aligned} f_1 = {} & \frac{a}{2}|\psi|^2 + b|\psi|^4 - \frac{c}{3}|\psi|^6 + 2\mathcal{K}|\mathbf{D}\psi|^2 \\ & - Q\left\{\left|\mathbf{D}^2\psi|^2 + \frac{1}{3}(\mathrm{rot}\mathbf{B}\cdot\mathbf{i}) + \frac{4e^2}{\hbar^2c^2}\mathbf{B}^2\right||\psi|^2\right\} \\ & - \frac{\mathcal{L}}{2}\{8|\psi|^2|\mathbf{D}\psi|^2 + [\psi^2(\mathbf{D}^*\psi^*)^2 + \text{c. c. }]\} \end{aligned} \tag{4}$$

where $\mathbf{i} = 4e\mathrm{Im}[\psi^*\mathbf{D}\psi]/\hbar c$. Coefficients $a, b, c, \mathcal{K}, \mathcal{L}$, and Q in this expansion depend on the chosen microscopic model for the single-particle states. Notice that f_1 depends only on the solution of the GL equations ψ and $\mathbf{B}$. The free energy provides one the criterium to find the most energetically favorable mixed-state configuration.

For practical calculations, it is more convenient to use the Gibbs energy with the density given as $g = f - \mathbf{H}\mathcal{B}/4\pi$, where $\mathbf{H}$ is the external magnetic field. We calculate the energy assuming $\mathcal{B}||\mathbf{H}$ are directed along the z axis and that external field H is equal to the thermodynamic critical field H_c. Notice that the value of H is irrelevant when the total magnetic flux through the sample is fixed. For convenience, we subtract the Gibbs energy of the uniform Meissner state from the result.

Finally, we write the resulting Gibbs energy (difference) using natural dimensionless quantities of the problem

$$\tilde{\mathbf{r}} = \frac{\mathbf{r}}{\lambda_L\sqrt{2}}, \tilde{\mathbf{B}} = \kappa\sqrt{2}\frac{\mathbf{B}}{H_c}, \tilde{\psi} = \frac{\psi}{\psi_0}$$

where $\psi_0 = \sqrt{|a|/b}$ is the order parameter in the uniform Meissner state, H_c is the thermodynamic critical field, λ_L is the magnetic penetration length, and $\kappa = \lambda_L/\xi$, with ξ the order parameter coherence length, all defined within the GL theory as

$$H_c = \sqrt{\frac{4\pi a^2}{b}}, \lambda_L^2 = \frac{\hbar^2c^2b}{32\pi e^2\mathcal{K}|a|}, \kappa = \frac{\lambda_L|a|}{\mathcal{K}}$$

Furthermore, to investigate the IT regime in the vicinity of the B-point (κ_0, T_c) we consider a further perturbation expansion of the Gibbs energy with respect to the deviation $\delta\kappa = \kappa - \kappa_0$, where we keep only the leading order contribution. After some (complicated) algebraic manipulations, the final expression for the Gibbs energy difference assumes a simple form[20]

$$\frac{G}{G_0} = -\frac{\delta\kappa}{\kappa_0}\mathcal{I} + \tau[c_{\mathcal{I}}\mathcal{I} + c_{\mathcal{J}}\mathcal{J}] \tag{5}$$

where the energy scale is $G_0 = \tau^2H_c^2L\lambda_L^2/4\pi$, L is the sample length in the z direction, and the constants read as

https://doi.org/10.1021/acs.jpclett.3c00721
J. Phys. Chem. Lett. 2023, 14, 3743−3748

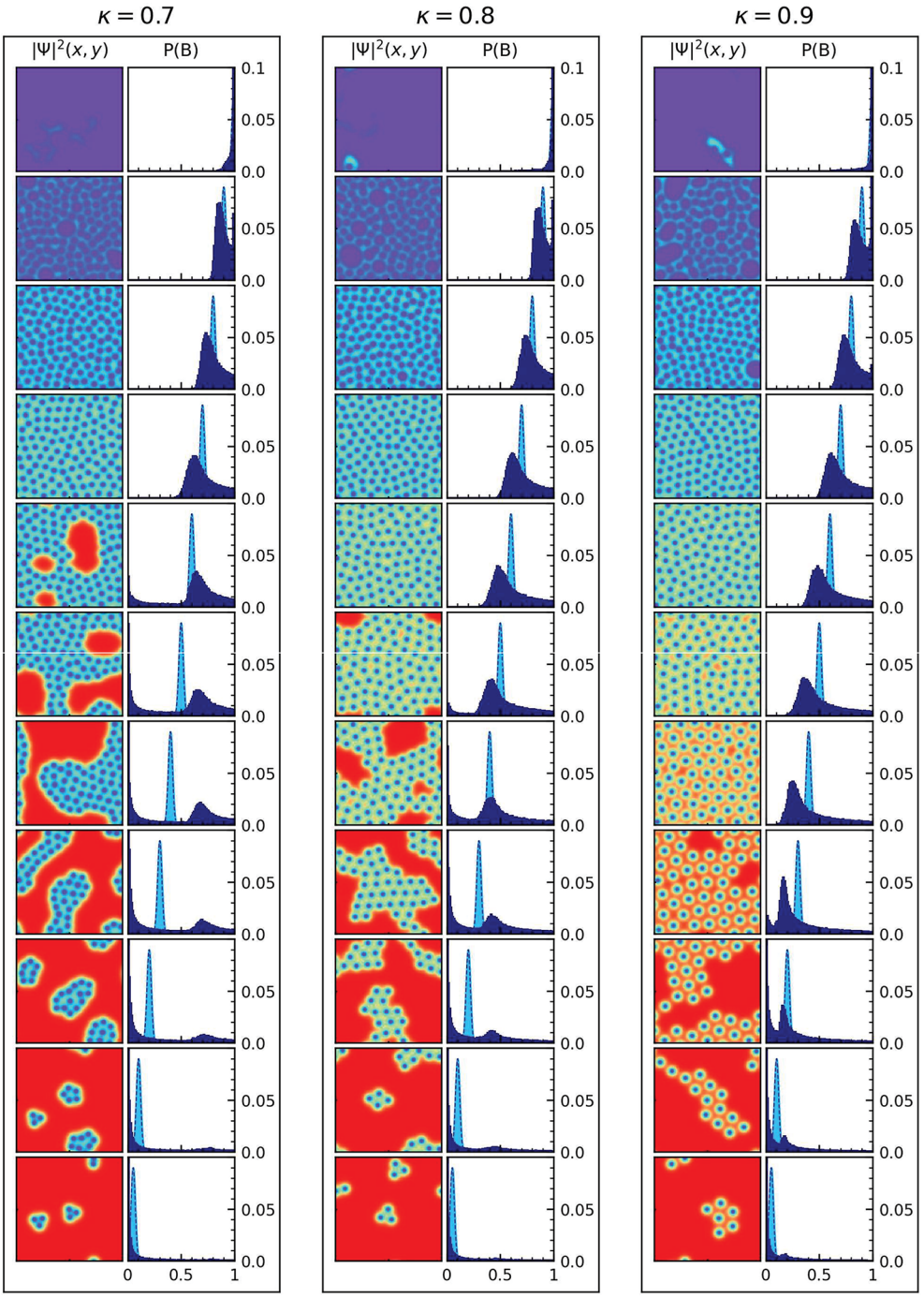

Figure 1. Color density plots show spatial profiles of the order parameter $|\psi|^2$ with the IMS vortex structure. Panels to the right of the color density plots give the sample-averaged magnetic flux distribution $P(B)$ (filled with dark blue color), sharp light-blue peaks indicate the sample average value of the magnetic field. The average field increases toward upper panels. The calculations are done for $\kappa = 0.7, 0.8, 0.9$, shown in three double-panel columns.

$$c_{\mathcal{I}} = 1 - \frac{c|a|}{3b^2} + 2\frac{\mathcal{Q}|a|}{\mathcal{K}^2}$$
$$c_{\mathcal{J}} = \frac{2\mathcal{L}|a|}{b\mathcal{K}} - \frac{c|a|}{3b^2} + \frac{5}{3}\frac{\mathcal{Q}|a|}{\mathcal{K}^2} \quad (6)$$

Quantities $\mathcal{I}$ and $\mathcal{J}$ are found as integrals

$$\mathcal{I} = \int \left|\psi|^2(1 - |\psi|^2)\right. \mathrm{d}^2\mathbf{r}$$
$$\mathcal{J} = \int \left|\psi|^4(1 - |\psi|^2)\right. \mathrm{d}^2\mathbf{r} \quad (7)$$

with ψ being the solution of the dimensionless GL equations at the Bpoint

$$-\mathbf{D}^2\psi - \psi(1 - |\psi|^2) = 0, \ \mathbf{rotB} = \mathbf{j} \quad (8)$$

and $\mathbf{D} = \nabla - i\mathbf{A}$. These equations can be solved for an arbitrary configuration of N vortices with cores located at $\mathbf{r}_j$ with $j = 1...N$. The solution to these equations is found using their self-duality, which yields $B = 1 - |\psi|^2$.[20,28] Vortex positions are regarded as variables, so that $\mathcal{I}$, $\mathcal{J}$, and energy G are functions of $\mathbf{r}_j$. It is worth noting that the result in eqs 5−(8) for the Gibbs energy in general holds for multiband superconductors as well.[20,28,44]

https://doi.org/10.1021/acs.jpclett.3c00721
J. Phys. Chem. Lett. 2023, 14, 3743−3748

Notice that coefficients $c_{\mathcal{I}}$ and $c_{\mathcal{J}}$ are obtained from the microscopical model of the single particle states in the material. A simple model with the spherical Fermi surface yields $c_{\mathcal{I}} = 0.41$ and $c_{\mathcal{J}} = 0.68$ independent of the microscopic parameters. However, due to the linear dependence of G on τ and $\delta\kappa$, qualitative properties of vortex configurations do not depend on particular values of $c_{\mathcal{I}}$ and $c_{\mathcal{J}}$ for as long as $c_{\mathcal{J}} > 0$. If this condition is satisfied, the IT superconductivity occupies a finite domain on the phase diagram, and its dimensions at different constant values are found by a simple scaling.[20,28]

To find the flux configuration with the minimal energy, we minimize G in eq 5 with respect to vortex positions $\mathbf{r}_j$ using the Metropolis algorithm, where we vary positions of vortices one by one and accept or reject the vortex movement using a chosen criterium. Details of both solving the GL equations and the Metropolis algorithm can be found elsewhere.[20,28]

Obtained spatial distributions of the order parameter $|\psi|^2$ are illustrated by color density plot panels in Figure 1. Upper panels correspond to larger values of the average magnetic field (proportional to the total magnetic flux or number N vortices in the sample). The uppermost panels correspond to the critical field where $|\psi|^2 = 0$ and superconductivity ceases.

Numerical calculations are performed for three values of the GL parameter $\kappa = 0.7, 0.8, 0.9$, representing different points in the phase diagram of superconductivity types (see ref 28). For all chosen κ the system is in the IT domain, but at $\kappa = 0.9$ it is close to the type II superconductivity, whereas at $\kappa = 0.7$, it shifts toward the type I regime. For clarity, we assume $\tau = 1$, utilizing the linear scaling dependence in eq 5.

For all considered values of κ, vortices form clusters at low values of the total flux. When the flux increases, sizes of the clusters grow, until vortices occupy the entire sample. This sequence of transformations takes place for all considered values of κ. In earlier works, it was named a hallmark of the IT superconductivity.[28,32−35]

We now correspond the spatial profile to the sample-averaged magnetic field distribution calculated using

$$P(B) = \sum_{\mathbf{r}} \delta(B - B(\mathbf{r})) \tag{9}$$

In our calculations, the magnetic field is found from the order parameter using the self-duality relation $B(\mathbf{r}) = 1 - |\psi(\mathbf{r})|^2$. Obtained distributions $P(B)$ are shown in panels to the right of the corresponding color density plots for the order parameter profile in Figure 1. The average value $\overline{B}$ of the magnetic field penetrating the sample is given by the position of a sharp light-blue peak.

Comparing right and left panels in Figure 1 demonstrates that changes in the vortex distribution and in $P(B)$ are connected. Existence of the Meissner phase in the order parameter profile is connected to a sharp peak in $P(B)$ at $B = 0$. Appearance of vortex clusters is related to a peak at finite field $B = B^*$.

When the average field $\overline{B}$ increases, the amplitude $P(0)$ of the first peak drops, while that of the second peak $P(B^*)$ rises. However, positions of both peaks, at $B = 0$ and B^*, do not change. This is understood by noting that, while sizes of vortex clusters increase, the average distance between vortices inside them is fixed. The amplitudes of the peaks indicate the relative areas occupied by vortex clusters and the Meissner phase.

The situation changes qualitatively when the average field $\overline{B}$ over the sample reaches the average field B^* inside vortex clusters. At this point the Meissner phase together with the peak in $P(B)$ at $B = 0$ disappears, and vortex clusters merge into a global vortice structure. When $\overline{B}$ increases further, the average field in clusters and in the entire sample coincide $B^* \simeq \overline{B}$, and the position of the second peak in $P(B)$ increases with the applied field. This situation is typical for type II superconductors. The increasing field gradually suppresses the superconducting state. When the field reaches its upper critical value H_{c2} the superconductivity ceases, and the field distribution $P(B)$ has only a sharp (singular) peak at $B = H_{c2}$.

These sequential changes in the vortex structure and in the field distribution $P(B)$ are similar for all considered values of κ [cf. Figure 1]. However, one observes notable differences in the vortex configurations at different values of κ. At $\kappa = 0.9$ (close to type II) vortices inside clusters are arranged in a regular lattice, whereas at $\kappa = 0.7$ (close to type I) they form something like a liquid state. Obviously, the distribution $P(B)$ cannot reflect fine changes in the vortex structure inside clusters. However, the position B^* of the second peak shifts to the right when κ decreases, the system moves closer to typeI superconductivity, and vortices form a liquid state. Therefore, the place of the second peak in the interval $[0, H_{c2}]$ indicates the place of the system in the phase diagram of the superconductivity types. Close to type II superconductivity (larger κ), the second peak is close to the left side of the interval, whereas B^* approaching H_{c2} proves the system approaches the type I regime.

Concluding, our theoretical analysis of the magnetic field dependence of vortex configurations in IT superconductors demonstrates that the field distribution $P(B)$ offers a reliable indicator for the vortex clustering, which manifests itself in the two-peak structure in $P(B)$. The peak at $B = 0$ corresponds to the Meissner phase, while the other peak at $B^* \neq 0$ is due to the vortex clustering. Positions of the peaks do not change when the applied field grows, until vortices occupy the entire space. At this point, the Meissner phase together with the first peak in $P(B)$ disappear, while the second peak shifts to larger values following the increasing applied field. The position of the second peak B^*, at small values of the applied field $\overline{B}$, indicates the place an IT superconductor on the phase diagram of superconductivity types, measuring how close (or far) the system is from the type I and type II superconductivity regimes. Finally, we stress that our analysis is universal and applies to multiband superconductors.

AUTHOR INFORMATION

Corresponding Author

A. Vagov − *HSE University, Moscow 101000, Russia; Moscow Institute of Physics and Technology, 141700 Dolgoprudny, Russia;* orcid.org/0000-0001-7446-7728; Email: av.vagov@hse.ru

Author

E.G. Nikonov − *Joint Institute for Nuclear Research, Dubna 141980, Russia; HSE University, Moscow 101000, Russia*

Complete contact information is available at: https://pubs.acs.org/10.1021/acs.jpclett.3c00721

ACKNOWLEDGMENTS

The authours gratefully acknowledge support from the Basic Research Program of the HSE University used to investigate vortex configurations. The work was also partially supported by the Ministry of Science and Higher Education of the Russian Federation (No. FSMG-2023-0014) and the RSF grant 23-72-30004.

REFERENCES

(1) Jena, P. Beyond the Periodic Table of Elements: The Role of Superatoms. *J. Phys. Chem. Lett.* **2013**, *4*, 1432−1442.
(2) Reed, C. A.; Bolskar, R. D. Discrete Fulleride Anions and Fullerenium Cations. *Chem. Rev.* **2000**, *100*, 1075−1120.
(3) Joshi, C. P.; Bootharaju, M. S.; Bakr, O. M. Tuning Properties in Silver Clusters. *J. Phys. Chem. Lett.* **2015**, *6*, 3023−3035.
(4) Chen, X.; Chen, D.; Weng, M.; Jiang, Y.; Wei, G.-W.; Pan, F. Topology-Based Machine Learning Strategy for Cluster Structure Prediction. *J. Phys. Chem. Lett.* **2020**, *11*, 4392−4401.
(5) Kasuya, A.; Sivamohan, R.; Barnakov, Y. A.; Dmitruk, I. M.; Nirasawa, T.; Romanyuk, V. R.; Kumar, V.; Mamykin, S. V.; Tohji, K.; Jeyadevan, B.; et al. Ultra-Stable Nanoparticles of CdSe Revealed from Mass Spectrometry. *Nat. Mater.* **2004**, *3*, 99−102.
(6) Zhang, B.; Zhu, T.; Ou, M.; Rowell, N.; Fan, H.; Han, J.; Tan, L.; Dove, M. T.; Ren, Y.; Zuo, X.; et al. Thermally-Induced Reversible Structural Isomerization in Colloidal Semiconductor CdS Magic-Size Clusters. *Nature Commun.* **2018**, *9*, 2499.
(7) Luan, C.; Gokcinar, O. O; Rowell, N.; Kreouzis, T.; Han, S.; Zhang, M.; Fan, H.; Yu, K. Evolution of Two Types of CdTe MagicSize Clusters from A Single Induction Period Sample. *J. Phys. Chem. Lett.* **2018**, *9*, 5288−5295.
(8) Zhang, J.; Hao, X.; Rowell, N.; Kreouzis, T.; Han, S.; Fan, H.; Zhang, C.; Hu, C.; Zhang, M.; Yu, K. Individual Pathways in the Formation of Magic-Size Clusters and Conventional Quantum Dots. *J. Phys. Chem. Lett.* **2018**, *9*, 3660−3666.
(9) Zhu, D.; Hui, J.; Rowell, N.; Liu, Y.; Chen, Q. Y.; Steegemans, T.; Fan, H.; Zhang, M.; Yu, K. Interpreting the Ultraviolet Absorption in the Spectrum of 415 nm-Bandgap CdSe Magic-Size Clusters. *J. Phys. Chem. Lett.* **2018**, *9*, 2818−2824.
(10) Lietard, A.; Verlet, J. R. R. Selectivity in Electron Attachment to Water Clusters. *J. Phys. Chem. Lett.* **2019**, *10*, 1180−1184.
(11) Zhang, J.; Baxter, E. T.; Nguyen, M.-T.; Prabhakaran, V.; Rousseau, R.; Johnson, G. E.; Glezakou, V.-A. Structure and Stability of the Ionic Liquid Clusters [EMIM]n[BF4]n+1 - (n = 1 - 9): Implications for Electrochemical Separations. *J. Phys. Chem. Lett.* **2020**, *11*, 6844−6851.
(12) Lushchikova, O. V.; Huitema, D. M. M.; López-Tarifa, P.; Visscher, L.; Jamshidi, Z.; Bakker, J. M. Structures of Cun+ (n = 3 - 10) Clusters Obtained by Infrared Action Spectroscopy. *J. Phys. Chem. Lett.* **2019**, *10*, 2151−2155.
(13) Rafelski, J. Melting Hadrons, Boiling Quarks. In *Melting Hadrons, Boiling Quarks - From Hagedorn Temperature to UltraRelativistic Heavy-Ion Collisions at CERN;* Rafelski, J., Ed.; Springer: Cham, Switzerland, 2016.
(14) Nikonov, E. G.; Shanenko, A. A.; Toneev, V. D. A Mixed Phase Model and the Softest Point Effect. *arXiv* **1998**, 89−122.
(15) Biro, T. S.; Shanenko, A. A.; Toneev, V. D. Toward Thermodynamic Consistency of Quasiparticle Picture. *Phys. At. Nucl.* **2003**, *66*, 982−996.
(16) Peppernick, S. J.; Dasitha Gunaratne, K. D.; Castleman, A. W., Jr. Towards Comprehending the Superatomic State of Matter. *Chem. Phys. Lett.* **2010**, *489*, 1−11.
(17) Jena, P.; Sun, Q. Super Atomic Clusters: Design Rules and Potential for Building Blocks of Materials. *Chem. Rev.* **2018**, *118*, 5755−5870.
(18) Castleman, A. W., Jr. From Elements to Clusters: The Periodic Table Revisited. *J. Phys. Chem. Lett.* **2011**, *2*, 1062−1069.
(19) Brandt, E. H.; Das, M. P. J. Supercond. *Nov. Magn.* **2011**, *24*, 57.
(20) Vagov, A.; Shanenko, A. A.; Milosevic, M. V.; Axt, V. M.; Vinokur, V. M.; Aguiar, J. A.; Peeters, F. M. Superconductivity between Standard Types: Multiband versus Single-band Materials. *Phys. Rev. B* **2016**, *93*, 174503.
(21) Auer, J.; Ullmaier, H. Magnetic Behavior of Type-II Superconductors with Small Ginzburg-Landau Parameters. *Phys. Rev. B* **1973**, *7*, 136.
(22) Krägeloh, U. Flux Line Lattices in the Intermediate State of Superconductors with Ginzburg-Landau Parameters near $1/\sqrt{2}$. *Phys. Lett. A* **1969**, *28*, 657−658.
(23) Essmann, U. Observation of the Mixed State. *Physica* **1971**, *55*, 83−93.
(24) Aston, D. R.; Dubeck, L. W.; Rothwarf, F. "Intermediate Mixed" State of Type-II Superconductors. *Phys. Rev. B* **1971**, *3*, 2231.
(25) Laver, M.; Forgan, E. M.; Brown, S. P.; Charalambous, D.; Fort, D.; Bowell, C.; Ramos, S.; Lycett, R. J.; Christen, D. K.; Kohlbrecher, J.; Dewhurst, C. D.; Cubitt, R. Spontaneous Symmetry-Breaking Vortex Lattice Transitions in Pure Niobium. *Phys. Rev. Lett.* **2006**, *96*, 167002.
(26) Klein, U. Microscopic Calculations on the Vortex State in Type II Superconductors. *J. Low Temp. Phys.* **1987**, *69*, 1−36.
(27) Miranović, P.; Machida, K. Thermodynamics and Magnetic Field Profiles in Low-? Type-II Superconductors. *Phys. Rev. B* **2003**, *67*, 092506.
(28) Vagov, A.; Wolf, S.; Croitoru, M. D.; Shanenko, A. A. Universal Flux Patterns and Their Interchange in Superconductors Between Types I and II. *Commun. Phys.* **2020**, *3*, 58.
(29) Wolf, S.; Vagov, A.; Shanenko, A. A.; Axt, V. M.; Aguiar, J. A. Vortex Matter Stabilized by Many-Body Interactions. *Phys. Rev. B* **2017**, *96*, 144515.
(30) Gutierrez, J.-Y.; Ge, J.; Lyashchenko, A.; Filipov, V.; Li, J.; Moshchalkov, V. V. Direct Visualization of Vortex Pattern Transition in ZrB_12 with Ginzburg-Landau Parameter Close to the Dual Point. *Phys. Rev. B* **2014**, *90*, 184511.
(31) Bogomolnyi, E. B. The Stability of Classical Solutions. *Sov. J. Nucl. Phys.* **1976**, *24*, 449−454.
(32) Mühlbauer, S.; Pfleiderer, C.; Böni, P.; Laver, M.; Forgan, E. M.; Fort, D.; Keiderling, U.; Behr, G. Morphology of the Superconducting Vortex Lattice in Ultrapure Niobium. *Phys. Rev. Lett.* **2009**, *102*, 136408.
(33) Reimann, T.; Schulz, M.; Mildner, D. F. R.; Bleuel, M.; Brulet, A.; Harti, R. P.; Benka, G.; Bauer, A.; Boni, P.; Muhlbauer, S. Domain Formation in the Type-II/1 Superconductor Niobium: Interplay of Pinning, Geometry, and Attractive Vortex-Vortex Interaction. *Phys. Rev. B* **2017**, *96*, 144506.
(34) Backs, A.; Schulz, M.; Pipich, V.; Kleinhans, M.; Boni, P.; Muhlbauer, S. Universal Behavior of the Intermediate Mixed State Domain Formation in Superconducting Niobium. *Phys. Rev. B* **2019**, *100*, 064503.
(35) Brems, X. S; Muhlbauer, S.; Cordoba-Camacho, W. Y; Shanenko, A. A; Vagov, A.; Albino Aguiar, J.; Cubitt, R. Current-Induced Self-Organisation of Mixed Superconducting States. *Supercond. Sci. Technol.* **2022**, *35*, 035003.
(36) Kirschner, F. K. K.; Sluchanko, N. E.; Filipov, V. B.; Pratt, F. L.; Baines, C.; Shitsevalova, N. Yu.; Blundell, S. Observation of a Crossover from Nodal to Gapped Superconductivity in $Lu_xZr_{1-x}B_{12}$. *Phys. Rev. B* **2018**, *98*, 094505.
(37) Biswas, P. K.; Rybakov, F. N.; Singh, R. P.; Mukherjee, S.; Parzyk, N.; Balakrishnan, G.; Lees, M. R.; Dewhurst, C. D.; Babaev, E.; Hillier, A. D.; Paul, D. M. K. Coexistence of Type-I and Type-II Superconductivity Signatures in ZrB_{12} Probed by Muon Spin Rotation Measurements. *Phys. Rev. B* **2020**, *102*, 144523.
(38) Babaev, E.; Carlstrom, J.; Speight, M. Type-1.5 Superconducting State from an Intrinsic Proximity Effect in Two-Band Superconductors. *Phys. Rev. Lett.* **2010**, *105*, 067003.
(39) Tsindlekht, M. I.; Leviev, G. I.; Genkin, V. M.; Felner, I.; Paderno, Y. B.; Filippov, V. B. Glasslike low-frequency ac response of ZrB_{12} and *Nb* single crystals in the surface superconducting state. *Phys. Rev. B* **2006**, *73*, 104507.
(40) Sluchanko, N.; Gavrilkin, S.; Mitsen, K.; Kuznetsov, A.; Sannikov, I.; Glushkov, V.; Demishev, S.; Azarevich, A.; Bogach, A.; Lyashenko, A.; Dukhnenko, A.; Filipov, V.; Gabani, S.; Flachbart, K.; Vanacken, J.; Zhang, G.; Moshchalkov, V. Superconductivity in ZrB and LuB with Various Boron Isotopes. *J. Supercond. Nov. Magn.* **2013**, *26*, 1663−1667.
(41) Wang, Y.; Lortz, R.; Paderno, Y.; Filippov, V.; Abe, S.; Tutsch, U.; Junod, A. Specific heat and magnetization of a ZrB_{12} Single Crystal: Characterization of a Type-II/1 Superconductor. *Phys. Rev. B* **2005**, *72*, 024548.

https://doi.org/10.1021/acs.jpclett.3c00721
J. Phys. Chem. Lett. 2023, 14, 3743−3748

(42) Lukyanchuk, I.; Vinokur, V. M.; Rydh, A.; Xie, R.; Milošević, M. V.; Welp, U.; Zach, M.; Xiao, Z. L.; Crabtree, G. W.; Bending, S. J.; Peeters, F. M.; Kwok, W. K. Rayleigh Instability of Confined Vortex Droplets in Critical Superconductors. *Nat. Phys.* **2015**, *11*, 21−25.
(43) da Silva, R. M.; Milošević, M. V.; Shanenko, A. A.; Peeters, F. M.; Aguiar, J. A. Giant Paramagnetic Meissner Effect in Multiband Superconductors. *Sci. Rep.* **2015**, *5*, 12695.
(44) Saraiva, T. T.; Cavalcanti, P. J. F.; Vagov, A.; Vasenko, A. S.; Perali, A.; Dell'Anna, L.; Shanenko, A. A. Multiband Material with a Quasi-1D Band as a Robust High-Temperature Superconductor. *Phys. Rev. Lett.* **2020**, *125*, 217003.

https://doi.org/10.1021/acs.jpclett.3c00721
J. Phys. Chem. Lett. 2023, 14, 3743−3748